Journal of Fluids and Structures (2001) **15,** 1137–1152
doi:10.1006/jfls.2001.0396, available online at http://www.idealibrary.com on IDEAL®

STABILITY ISSUES OF CONCENTRIC PIPES CONTAINING STEADY AND PULSATILE FLOWS

X. WANG

Department of Mechanical Engineering, Polytechnic University
Brooklyn, NY 11201, U.S.A.

AND

F. BLOOM

Department of Mathematical Sciences, Northern Illinois University
DeKalb, IL 60115, U.S.A.

(Received 15 February 1999, and in final form 2 February 2000)

In this paper, we study both the static and dynamic instabilities of submerged and inclined concentric pipes conveying fluid. The governing equation for the inner tubular beam is derived under small deformation assumptions. We obtain the discretized dynamical equations using spatial finite-difference schemes. In the case of steady flow, both buckling and flutter instabilities are investigated. In the case of pulsatile flow, we compute the eigenvalues of the monodromy matrix derived from the discretized linear system with periodic coefficients, and deduce the dynamical stability information. In addition, for a special case, in which the concentric pipes have the same length, we compare the dynamic stability results with the corresponding solutions obtained with the Bolotin method.

1. INTRODUCTION

FLUID-CONVEYING PIPES ARE widely used in engineering applications. One of the design challenges is to avoid pipe buckling and flutter under various operation conditions. Initial work on such flow-induced vibration analysis was reported by Ashley & Haviland (1950), Benjamin (1961*a*, *b*), and Païdoussis (1966). A recent survey of this subject is available in Païdoussis & Li (1993) and Païdoussis (1998).

In the paper industry, one of the key components in approach flow systems (fiber stock delivery systems to paper machines) is the so-called silo water-mixing unit, a cylindrical water storage tank with a constant water level, as depicted in Figure 1. The inner pipe protruding into the fan pump inlet zone contains a higher consistency fiber stock, and the concentric outer pipe collects the recirculated stock. In addition to the effects on the smooth operation of impellers, the uniformity of stock consistency, and the minimization of pressure variations (Wang *et al*., 1999), the turbulent jets coming out of the concentric pipes may introduce severe oscillations in the suspended pipes, which can cause structural damages such as fatigue failure of pipe joints. The flow-induced oscillations associated with the submerged and inclined concentric pipes have been studied by Wang & Bloom (1999), in which the effects of various design parameters on the natural frequencies and damping ratios are discussed.

In this paper, we consider the stability issues related to such pipe systems. In addition to the divergence (buckling) and oscillatory (flutter) instabilities, we also consider the possible

0889–9746/01/081137 + 16 $35.00/0

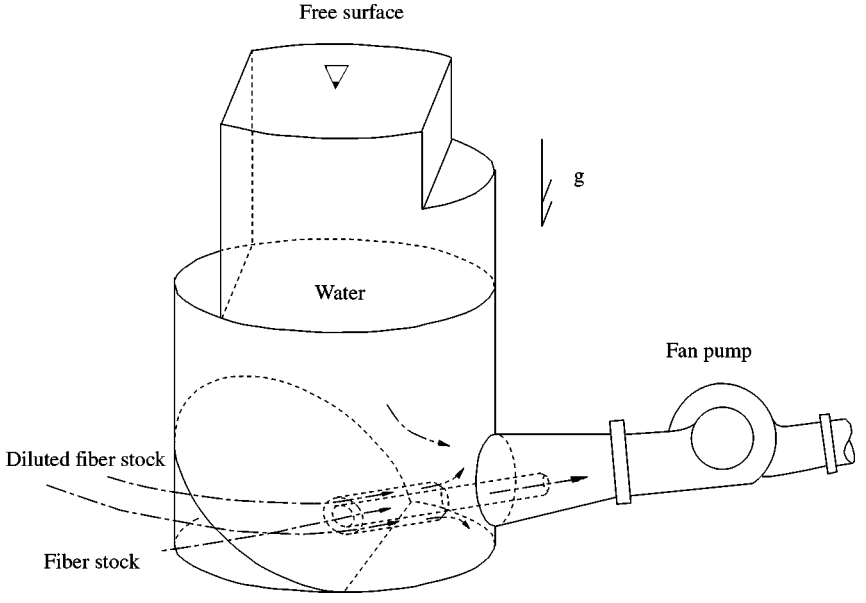

Figure 1. Location of the mixing pipe in the silo unit.

dynamic instability induced by a pulsating flow (Chen 1971; Païdoussis & Issid 1974). Apart from the traditional approach of the Galerkin–Ritz method, with one or two terms for the spatial series expansions, and the Bolotin method (Bolotin 1964), we incorporate, in this work, the spatial finite difference approach presented by Wang & Bloom (1999) along with a direct time integration for the computation of the monodromy matrix. The advantage of finite-difference schemes is to avoid the use of C^1 finite elements or mixed formulations. An elaborate discussion on this subject is available in Bathe (1996) and Zienkiewicz (1977). Based on the eigenvalues of the monodromy matrix, we then deduce the dynamic stability information corresponding to the presence of periodic coefficients. Of course, the physical problem discussed in this paper also possesses some novelty, in particular, discontinuous coefficients introduced by different pipe lengths.

We begin with the mathematical model and its corresponding governing equation in Section 2, and discuss the numerical procedures for the spatial discretization and the construction of the monodromy matrix in Section 3. We present in Section 4 numerical results for a particular pipe system design with both steady and pulsatile flows. As a further check on the numerical results obtained in Section 4, we also offer, in Section 5, an analytical study based on the Bolotin method to compare with the numerical Floquet approach, for a particular pipe system design.

2. THE MATHEMATICAL MODEL

Figure 2 shows the mathematical model of the suspended concentric pipe system with the longitudinal direction being that of the x-axis. We assume that the outer pipe is rigid and consider the inner pipe to be a tubular beam. We note that both pipes are submerged in water, and continuous flow between the two concentric cylinders only occurs in the domain $0 \leq x \leq L \leq l$. For the pulsatile inner pipe flow we have $U_i = \bar{U}_i(1 + \varepsilon \cos \omega_o t)$, where $\bar{U}_i$, ε, and ω_o represent the mean value of the averaged inner pipe flow velocity, the velocity perturbation magnitude, and the perturbation frequency, respectively. According to the

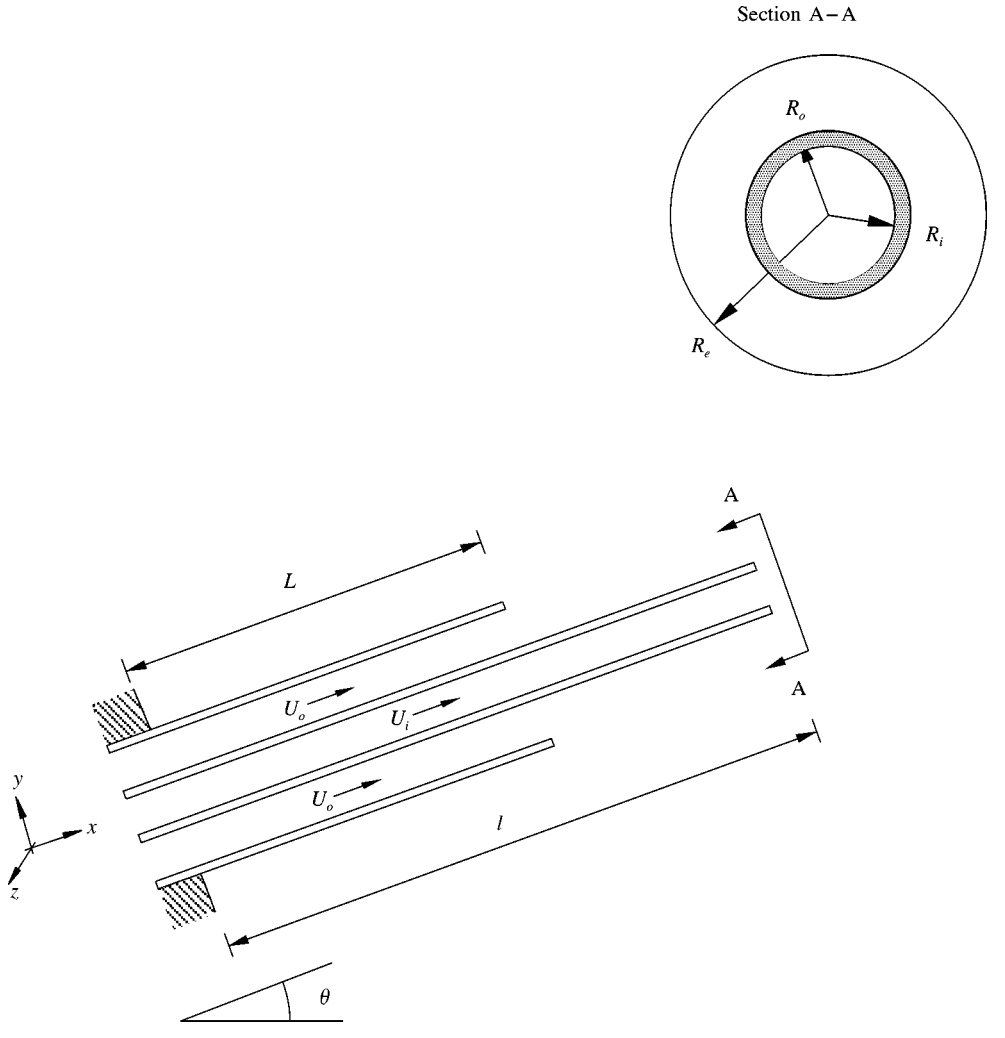

Figure 2. The mathematical model of the suspended concentric piping configuration.

discussion in Païdoussis & Issid (1974), the inertia term $\rho A_i(\partial U_i/\partial t)$ needs to be added to the axial force equilibrium of the internal flow. By the chain rule, we have for the transverse inertia effects

$$\left(\frac{\partial}{\partial t} + U_i \frac{\partial}{\partial x}\right)^2 = \frac{\partial^2}{\partial t^2} + 2U_i \frac{\partial^2}{\partial x \partial t} + U_i^2 \frac{\partial^2}{\partial x^2} + \frac{\partial U_i}{\partial t} \frac{\partial}{\partial x}. \tag{1}$$

Moreover, we denote the free surface level measured from the origin (0, 0) (fixed boundary location for the suspended pipes) as y_o, such that the hydrostatic pressure at the tip of the submerged beam ($x = l$) is given by $\bar{p} = \rho g y_o - \rho g l \sin\theta$; thus, we obtain the expression for the hydrostatic pressure of the external fluid:

$$p_e = (l - x)\rho g \sin\theta - y\rho g \cos\theta + \bar{p}. \tag{2}$$

According to Païdoussis (1973), Hannoyer & Païdoussis (1978), and Païdoussis & Pettigrew (1979), we also have the following expression for the hydrodynamic pressure in

the concentric flow region:

$$p_o A_o = \frac{1}{2}\rho D_o U_e^2 C_f h(x), \tag{3}$$

where the friction coefficient C_f has, as discussed by Taylor (1952), Païdoussis (1966), and Schlichting (1987), different values in the confined and unconfined regions, i.e.,

$$\mathrm{C}_f = \begin{cases} C_f^1, & 0 \le x < L, \\ C_f^2, & L \le x \le l, \end{cases} \tag{4}$$

while

$$h(x) = \begin{cases} \dfrac{R_o}{R_e - R_o}(L - x), & 0 \le x < L, \\ 0, & L \le x \le l, \end{cases} \tag{5}$$

and

$$\frac{\mathrm{d}h(x)}{\mathrm{d}x} = \begin{cases} -\dfrac{R_o}{R_e - R_o}, & 0 \le x < L, \\ 0, & L \le x \le l. \end{cases} \tag{6}$$

As discussed by Païdoussis (1966, 1973) and Hannoyer & Païdoussis (1978), the external flow exerts on the tubular beam (inner pipe) the following viscous forces per unit length in both transverse and longitudinal (axial) directions and more elaborate illustration of forces acting on the inner pipe is available in Wang & Bloom (1999):

$$f_x^e = \frac{1}{2}\rho D_o U_e^2 C_f, \qquad f_y^e = -\frac{1}{2}\rho D_o U_e C_f \left(\frac{\partial y}{\partial t} + U_e \frac{\partial y}{\partial x}\right), \tag{7}$$

where y stands for the transverse displacement of the tubular beam.

Defining the functions $\sigma = 1 + 0{\cdot}4(x_o/L)C_f^1$ and $\alpha = 0{\cdot}4C_f^1/\sigma$ for the confined external flow region, we obtain the external fluid inertia forces

$$\begin{aligned} \mathscr{F}_x^e &= 0, \\ \mathscr{F}_y^e &= -\chi\rho A_o \left(\frac{\partial}{\partial t} + \tilde{U}_e \frac{\partial}{\partial x}\right)\left(\frac{\partial}{\partial t} + U_e \frac{\partial}{\partial x}\right) y, \end{aligned} \tag{8}$$

where

$$\chi = \begin{cases} \dfrac{R_e^2 + R_o^2}{R_e^2 - R_o^2}, & 0 \le x < L, \\ 1, & L \le x \le l, \end{cases} \tag{9}$$

and

$$\tilde{U}_e = \begin{cases} U_e(1\text{-}\alpha(x/L)^2)/\sigma, & 0 \le x < L, \\ U_e, & L \le x \le l. \end{cases} \tag{10}$$

Following the derivation by Wang & Bloom (1999), we obtain the explicit expression for the tension T, based on the assumption that $p_i|_{x=l} = \bar{p} - \frac{1}{2}\rho D_o^2 U_e^2 C_b/A$, and the axial force equilibrium at the tip of the tubular beam, i.e., $T|_{x=l} = -\bar{p}A + \frac{1}{2}\rho D_o^2 U_e^2 C_b$, where C_b is the coefficient representing the base drag. Abbreviating $-\bar{p}A_o + \frac{1}{2}\rho D_o^2 U_e^2 C_b A_o/A$ as $\mathscr{G}_0$, $(m + \rho A_i)g\sin\theta + \rho A_i \partial U_i/\partial t$ as $\mathscr{G}_1$, and $\frac{1}{2}\rho D_o U_e^2$ as $\mathscr{G}_2$, with m as the mass per unit length

of the inner pipe, we obtain

$$\frac{\partial(T - p_i A_i)}{\partial x} = \mathscr{G}_1 - \mathscr{G}_2 C_f, \tag{11}$$

so that

$$\begin{aligned} T - p_i A_i &= \mathscr{G}_0 + (x - l)\mathscr{G}_1 + \mathscr{G}_2 \int_x^l C_f \, \mathrm{d}x \\ &= \mathscr{G}_0 + (x - l)\mathscr{G}_1 + \mathscr{G}_2 \begin{cases} C_f^1(L - x) + C_f^2(l - L), & 0 \le x < L, \\ C_f^2(l - x), & L \le x \le l. \end{cases} \end{aligned} \tag{12}$$

Thus, in a manner similar to the derivation presented by Wang & Bloom (1999), we find the following governing equation for $y(x, t)$:

$$c_1 \frac{\partial^4 y}{\partial x^4} + c_2 \frac{\partial^2 y}{\partial x^2} + c_3 \frac{\partial^2 y}{\partial x \partial t} + c_4 \frac{\partial^2 y}{\partial t^2} + c_5 \frac{\partial y}{\partial x} + c_6 \frac{\partial y}{\partial t} = 0, \tag{13}$$

where the coefficients are given by

$$\begin{aligned} c_1 &= EI, \\ c_2 &= \rho A_i U_i^2 - (T - p_i A_i + p_e A_o + \tfrac{1}{2}\rho D_o U_e^2 C_f h(x)) + \chi \rho A_o \tilde{U}_e U_e, \\ c_3 &= 2\rho A_i U_i + \chi \rho A_o (\tilde{U}_e + U_e), \\ c_4 &= m + \rho A_i + \chi \rho A_o, \\ c_5 &= -(m + \rho A_i - \rho A_o) g \sin\theta + \tfrac{1}{2}\rho D_o U_e^2 C_f \left(1 - \frac{\mathrm{d}h(x)}{\mathrm{d}x}\right), \\ c_6 &= \tfrac{1}{2}\rho D_o U_e C_f. \end{aligned} \tag{14}$$

Notice that for the case of a clamped (or built-in) boundary condition at $x = 0$, we have

$$y(0, t) = 0, \quad \frac{\partial y(0, t)}{\partial x} = 0, \tag{15}$$

while for the free end of the tubular beam at $x = l$, we have

$$\frac{\partial^2 y(l, t)}{\partial x^2} = 0, \quad EI \frac{\partial^3 y(l, t)}{\partial x^3} + \left(\bar{p} A - \frac{1}{2}\rho D_o^2 U_e^2 C_b\right) \frac{\partial y(l, t)}{\partial x} = 0. \tag{16}$$

We also recognize that the coefficients c_1 to c_6 can be variable depending on the position x. To circumvent the discontinuity at the location $x = L$, where the confined and unconfined external flow domains are separated, we prescribe a nodal point at that location. Of course, for pulsatile flow, only the coefficients c_2 and c_3 are periodic in time with the period $T_o = \omega_o/(2\pi)$.

Since we focus our attention on the stability issues, we only retain in equation (13) the homogeneous part of the governing equation.

3. STABILITY ANALYSIS

We employ the standard finite-difference discretizations to replace the partial differential equation (13) with a set of ordinary differential equations with respect to time. Equivalent difference schemes are also used for the boundary conditions in equations (15) and (16). We

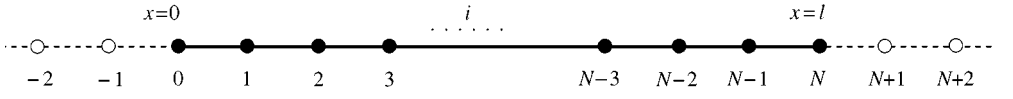

Figure 3. Finite difference stations on the tubular beam.

define the solution variable $y(x,t)$ at the spatial grid (or nodal) point i as $Y^i(t)$ (depicted in Figure 3), and its corresponding time derivative as $\dot{Y}^i(t)$. Using an equal spacing h between finite difference stations, and employing the same finite-difference approximations as used by Wang & Bloom (1999), we obtain the discretized characteristic equation for node i $(1 \le i \le N)$:

$$c_4^i \ddot{Y}^i + \frac{c_3^i}{2h}\dot{Y}^{i+1} - \frac{c_3^i}{2h}\dot{Y}^{i-1} + \frac{c_1^i}{h^4}Y^{i+2} + \left(\frac{c_2^i}{h^2} - \frac{4c_1^i}{h^4} + \frac{c_5^i}{2h}\right)Y^{i+1} + \left(\frac{6c_1^i}{h^4} - \frac{2c_2^i}{h^2}\right)Y^i + \left(\frac{c_2^i}{h^2} - \frac{4c_1^i}{h^4} - \frac{c_5^i}{2h}\right)Y^{i-1} + \frac{c_1^i}{h^4}Y^{i-2} + c_6^i \dot{Y}^i = 0. \quad (17)$$

As the variable coefficients c_1 to c_5 in (14) could be functions of x they are denoted as c_1^i to c_5^i at the nodal point i. Therefore, equation (13) becomes

$$\mathbf{M}\ddot{\mathbf{Y}} + \mathbf{C}\dot{\mathbf{Y}} + \mathbf{K}\mathbf{Y} = \mathbf{0}, \quad (18)$$

where $\mathbf{Y}$ is the solution vector, and $\mathbf{M}$, $\mathbf{C}$, and $\mathbf{K}$ stand for the mass, damping (including gyroscopic terms), and stiffness algebraic coefficient matrices, respectively. For the steady flow case, i.e., $\varepsilon = 0$, if we assume a characteristic solution $\mathbf{Y} = e^{i\omega t}\hat{\mathbf{Y}}$, where $\hat{\mathbf{Y}}$represents the mode shape with the natural frequency $\omega = 2\pi f$, the stable system corresponds to $\mathscr{I}m(\omega) \ge 0$ with $\mathscr{R}e(\omega) \ne 0$. We define the buckling instability as $\mathscr{R}e(\omega) \to 0$ with $\mathscr{I}m(\omega) \ge 0$, and the flutter instability as $\mathscr{I}m(\omega) < 0$ with $\mathscr{R}e(\omega) \ne 0$. Moreover, having the set of second-order ordinary differential equations in (18), for the case of pulsatile flow, we now introduce a new solution vector $\mathbf{q} = (\mathbf{Y}, \dot{\mathbf{Y}})$, and replace (18) with the following system of $2N$ first-order differential equations with periodic coefficients:

$$\dot{\mathbf{q}} = \mathbf{A}(t)\mathbf{q}, \quad (19)$$

where

$$\mathbf{A}(t) = \begin{bmatrix} \mathbf{0} & \mathbf{I} \\ -\mathbf{M}^{-1}\mathbf{K} & -\mathbf{M}^{-1}\mathbf{C} \end{bmatrix}.$$

Of course, the stability analysis of the trivial solution of equation (19) also applies to the stability of solutions near the fixed point of the nonlinear dynamical system with the Jacobian matrix $\mathbf{A}(t)$. For this nonautonomous system, the matrix $\mathbf{A}(t)$ has a period T_o. According to the Floquet theory, the fundamental matrix satisfying equation (19) can be expressed as the function of a periodic nonsingular matrix $\mathbf{Q}(t)$, with the period T_o, and a constant matrix $\mathbf{D}$,

$$\mathbf{q}(t) = \mathbf{Q}(t)e^{t\mathbf{D}}. \quad (20)$$

Therefore, the eigenvalues of the matrix $\mathbf{D}$, denoted by β, determine the stability of (19), and we obtain

$$\mathbf{q}(t + T_o) = \mathbf{q}(t)\mathbf{N}, \quad (21)$$

with the monodromy matrix $\mathbf{N} = e^{T_o\mathbf{D}}$.

The eigenvalues of the matrix **N**, denoted by λ, are related to the eigenvalues β of the matrix **D** by

$$\beta = \frac{1}{T_o}(\log|\lambda| + \mathrm{i}\arg\lambda), \quad \mathrm{i} = \sqrt{-1}. \tag{22}$$

It is clear that only the real part of β is uniquely defined. If we assign

$$\mathbf{q}(0) = \mathbf{I}, \tag{23}$$

where **I** is the identity matrix, we obtain

$$\mathbf{N} = \mathbf{q}(T_o). \tag{24}$$

In order to derive the monodromy matrix **N**, we numerically integrate equation (19), together with the initial condition (23), using the second-order Runge–Kutta method, i.e.,

$$\mathbf{q}(t + \Delta t) = \mathbf{q}(t) + \Delta t(\mathbf{k}_1 + \mathbf{k}_2)/2, \tag{25}$$

where

$$\mathbf{k}_1 = \mathbf{A}(t)\,\mathbf{q}(t),$$

$$\mathbf{k}_2 = \mathbf{A}(t + \Delta t)(\mathbf{q}(t) + \Delta t\,\mathbf{A}(t)\mathbf{q}(t)).$$

The ith column of the matrix **N** corresponds to the numerical solution of (19) with the ith column of the identity matrix **I** as the initial condition. In general, due to the explicit nature of the Runge–Kutta scheme, the construction of the monodromy matrix can be very expensive. The detailed discussion on the selection of a proper time step is presented by Wang & Hale (2001).

4. NUMERICAL RESULTS

We study the stability issues for a particular pipe system design with the following physical parameters: $\rho = 1000\,\mathrm{kg/m^3}$, $m = 2{\cdot}12\,\mathrm{kg/m^3}$, $l = 2{\cdot}392\,\mathrm{m}$, $L = 1{\cdot}135\,\mathrm{m}$, $x_o = 2{\cdot}4\,\mathrm{m}$, $y_o = 6{\cdot}155\,\mathrm{m}$, $R_i = 0{\cdot}02\,\mathrm{m}$, $R_o = 0{\cdot}025\,\mathrm{m}$, $R_e = 0{\cdot}035\,\mathrm{m}$, $g = 9{\cdot}8\,\mathrm{m/s^2}$, $E = 70\,\mathrm{GPa}$, $C_f^1 = 0{\cdot}004\pi$, $C_f^2 = 0{\cdot}5\pi R_i/l$, and $C_b = 0{\cdot}0125\pi$. Note that the selection of C_f^2 is based on the assumption in Païdoussis (1966). In particular, C_f^2 is defined as $c_T\pi/4$ according to Païdoussis (1966), and from the assumption in the same reference, εc_T is equal to 1, with $\varepsilon = 0{\cdot}5l/R_i$.

4.1. Steady-Flow Cases

For the steady-flow cases, Figure 4 shows the loci of the fourth mode in the complex ω plane as a function of the dimensionless velocity $u = \sqrt{\rho A_i/EI}\,U_i l$, i.e., $u = 0{\cdot}0238U_i$.

As illustrated in Figure 4, for the length ratio $L/l = 0{\cdot}4745$, without friction effects, there is a small flutter range, which disappears with the addition of friction terms. This indicates that friction forces have positive effects on avoiding flutter instability. Notice that the disappearance of the flutter does not occur in a different mode. In fact, we find that the fourth mode is the mode in which, for a sufficiently high value of u, flutter instability can occur. It is interesting to observe that higher modes are often more prone to flutter than lower modes. This phenomenon is consistent with the results in Païdoussis (1998), and moreover, stays the same as we vary the parameters.

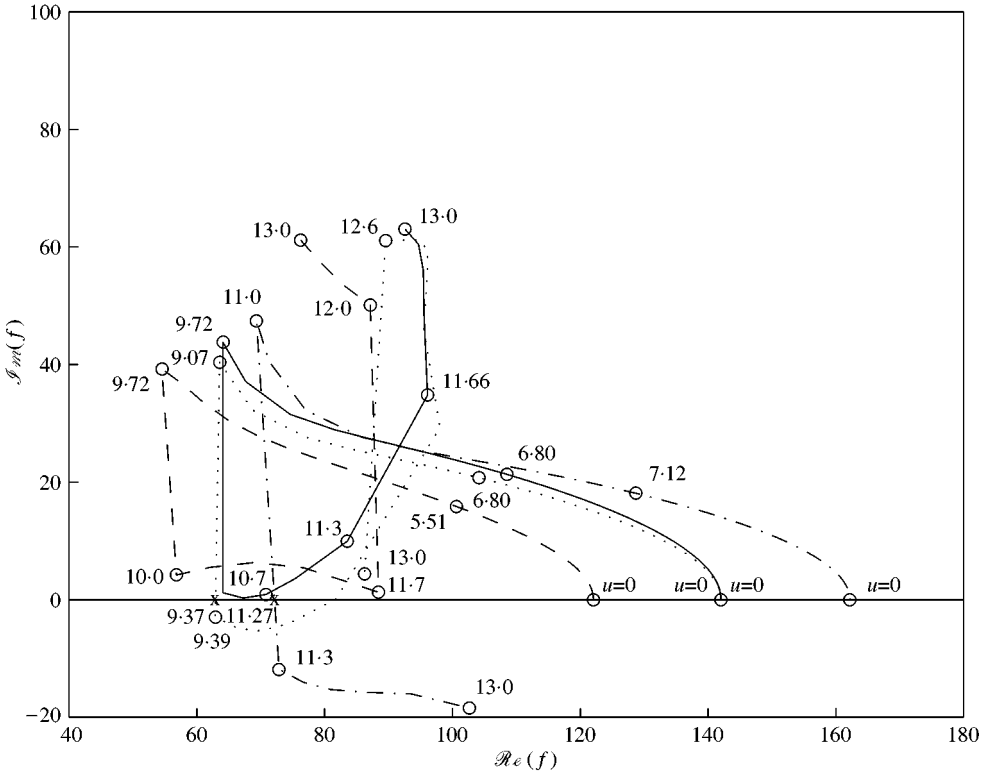

Figure 4. Flutter instability of the fourth mode with $U_i/U_e = 1{\cdot}7$. (Twenty-one grid points.) —, with friction effects, $L/\mathrm{I} = 0{\cdot}4745$; ---, without friction effects, $L/I = 0{\cdot}4745$, $u_c = 9{\cdot}37$; - - -, with friction effects, $L/I = 1$; -·-, without friction effects, $L/I = 0$, $u_c = 11{\cdot}27$.

In addition, Figure 4 also shows that the higher the inner and outer pipe length ratio, the less likely it is that flutter will occur, which might be attributed to frictional effects within the concentric flow region.

As depicted in Figure 5, we also reach the conclusion that friction forces have positive effects on delaying the buckling instability. However, the higher the inner and outer pipe length ratio, the more susceptible the inner pipe is to buckling. This is of course in contrast to the observation with respect to flutter instability and suggests that the length effects are more significant than the frictional effects.

Figure 5 also shows that as we approach the buckling points, the decreasing rate of the imaginary component of complex frequency becomes large, and more points are needed to obtain smooth curves around the buckling points.

A more elaborate study on the dependence of the critical buckling velocity u_c on the pipe length ratio, friction, and gravitational forces indicates, as shown in Figure 6, that there exists a transition region around $L/l = 0{\cdot}6$. Considering the fact that the natural frequency results in Wang & Bloom (1999) are smooth around $L/l = 0{\cdot}6$, we conjecture that the mode shape effect is unlikely to be the cause of the discontinuity. Nevertheless, the physical cause for such a discontinuity is still not clear.

Another important observation worth mentioning is that the effects of gravitational forces are not as significant as those of frictional forces; this fact is also consistent with the calculations of the natural frequencies presented in Wang & Bloom (1999).

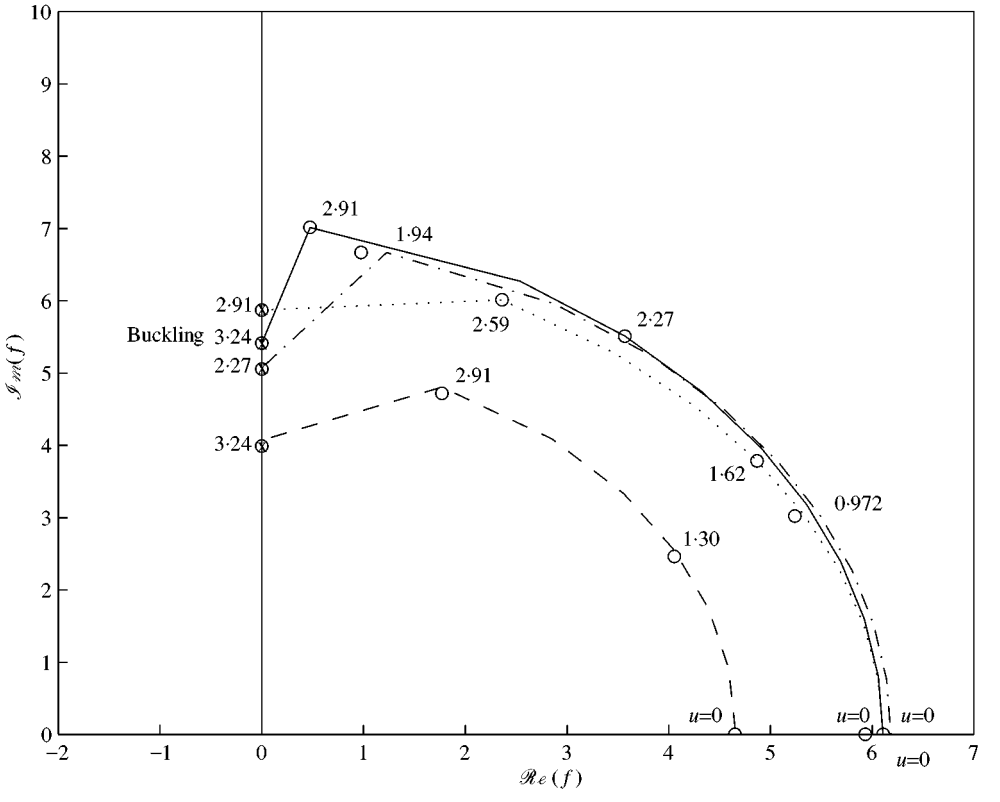

Figure 5. Buckling instability of the first mode with $U_i/U_e = 1{\cdot}7$. (Twenty-one grid points.) —, with friction effects, $L/\mathrm{I} = 0{\cdot}4745$, $u_c = 3{\cdot}24$ (×); ---, without friction effects, $L/I = 0{\cdot}4745$, $u_c = 2{\cdot}92$ (×); — —, with friction effects, $L/I = 1$, $u_c = 2.27$ (x); —, without friction effects, $L/I = 0$, $u_c = 3{\cdot}24$ (×).

4.2. Unsteady-Flow Cases

For the pulsatile-flow cases, we denote ω_{oi} as the ith natural frequency of the corresponding steady-flow case with both gravity and friction effects. As discussed by Païdoussis & Pettigrew (1979), Noah & Hopkins (1980) and Ariaratnam & Namachchivaya (1986), although the numerical Floquet analysis is lengthier than the Bolotin method with two expansion terms, it includes both the parametric ($\omega_o/\omega_{oi} = 2/k, \quad k = 1, 2, 3, \ldots$) and combination instabilities ($\omega_o/(\omega_{oi} - \omega_{oj}) = 1/k$, $k = 1, 2, 3, \ldots$), and is convenient to implement.

Figure 7 shows the dynamic instability regions for different cases. It is clear from the figure that the gravitational effects are not significant, which is consistent with the natural frequency calculations in Wang & Bloom (1999). In fact, in the dynamic stability analysis, both gravitational and friction effects are not as significant as the inner and outer pipe length ratio L/l. Notice that this dynamic instability result with respect to friction is quite different from the conclusion of the static instability analysis.

It is also interesting to note, based on Figure 7, that the combination instability in this case does not show up within the frequency range $1{\cdot}7\omega_{02} \sim 2{\cdot}7\omega_{02}$. Moreover, the dynamical instability or resonance is also selectively associated with only some of the modes, and the higher the perturbation, the more likely it is that the dynamical instability will occur.

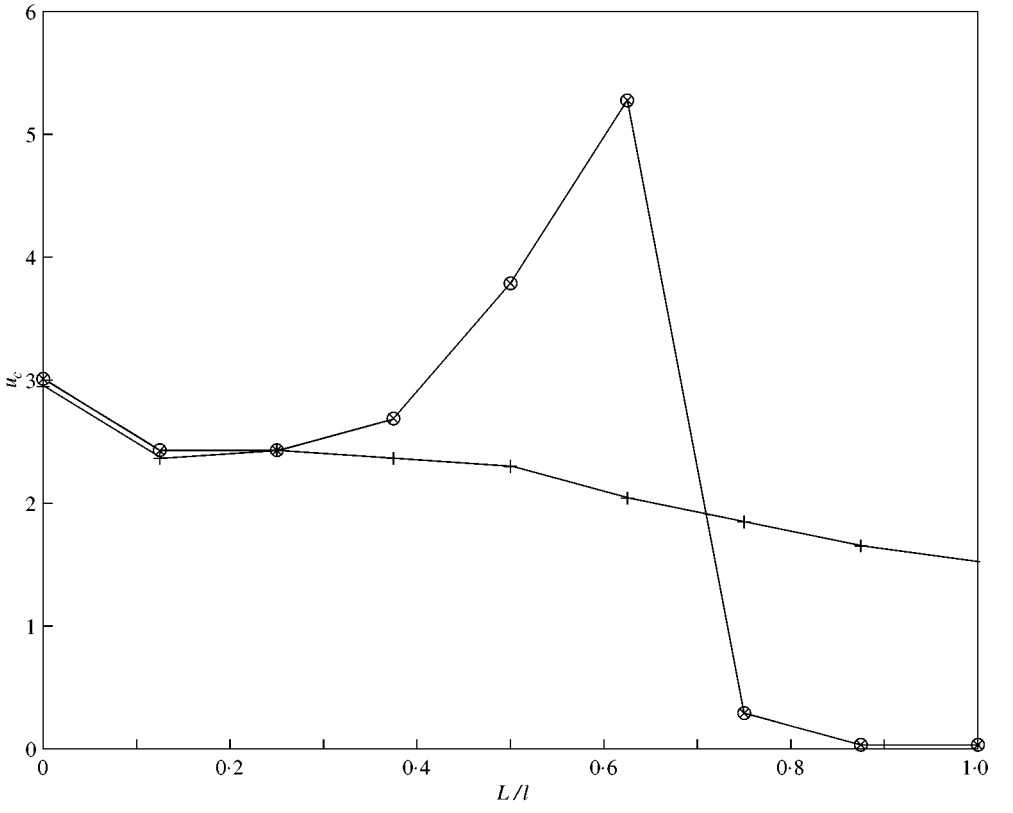

Figure 6. Critical buckling velocity versus the outer pipe length with $U_i/U_e = 1{\cdot}7$. (Twenty-one grid points.) +, without friction effects; ○, with gravity and friction effects; ×, without gravity effects.

5. BOLOTIN METHOD

In this section we consider the case of a pipe system with the same inner and outer pipe lengths. To simplify the expression for the eigenfunctions satisfying the beam equation and its associated boundary conditions, we ignore frictional forces, the axial load at the tip of the inner tubular beam, and, in general, the gravitational forces. As a consequence of equation (12), the forms of $\mathscr{G}_0$ and $\mathscr{G}_1$, and the assumed structure of the pulsatile inner pipe flow, we have

$$T - p_i A_i = (l - x)\rho A_i \bar{U}_i \omega_o \varepsilon \sin \omega_o t, \tag{26}$$

while the coefficients c_1 to c_6 in equation (14) take on the following form:

$$\begin{aligned} c_1 &= EI, \\ c_2 &= \rho A_i \bar{U}_i^2 (1 + \varepsilon \cos \omega_o t)^2 + (x - l)\rho A_i \bar{U}_i \omega_o \varepsilon \sin \omega_o t + \chi \rho A_o U_e^2, \\ c_3 &= 2\rho A_i \bar{U}_i (1 + \varepsilon \cos \omega_o t) + 2\chi \rho A_o U_e, \\ c_4 &= m + \rho A_i + \chi \rho A_o, \qquad c_5 = 0, \qquad c_6 = 0. \end{aligned} \tag{27}$$

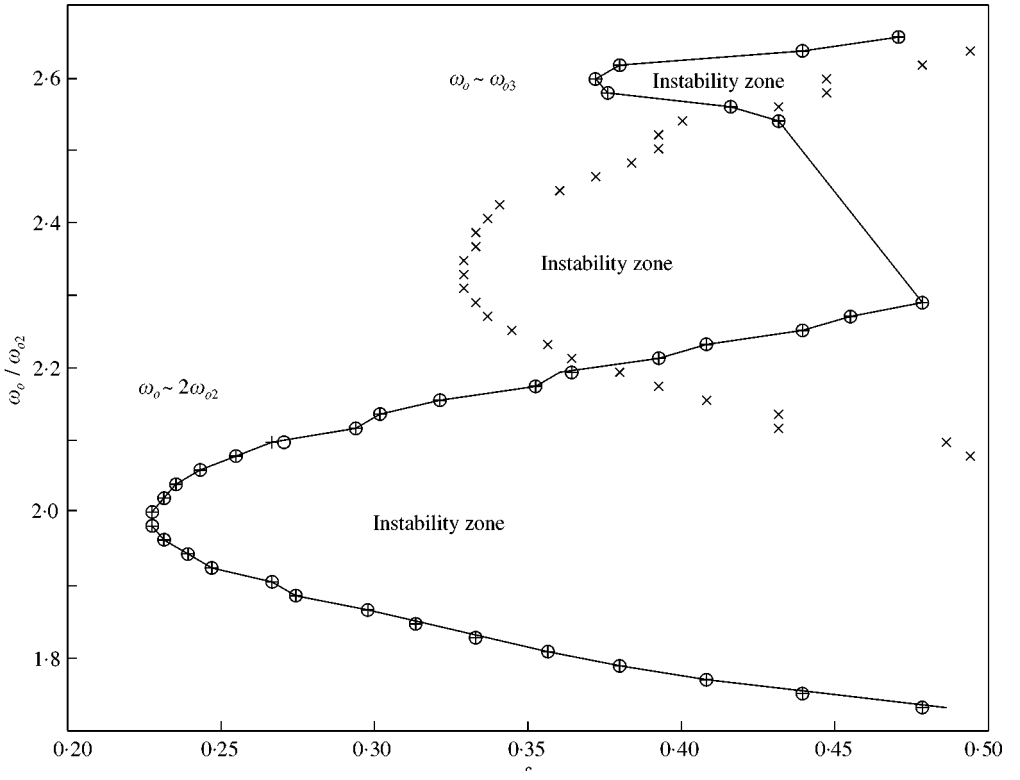

Figure 7. Dynamic instability regions. ($\omega_{o1} = 26{\cdot}13$ rad/s and $\omega_{o2} = 117{\cdot}3$ rad/s with five grid points.) —, $L/I = 1$; ×, $L/I = 0{\cdot}4745$; +, without friction effects; ○, without gravity effects.

In addition, we may rewrite c_2 and c_3 in the form

$$c_2 = \bar{c}_2 + \tilde{c}_2^1 \varepsilon \cos \omega_o t + (x - l)\tilde{c}_2^2 \varepsilon \sin \omega_o t + \tilde{c}_2^3 \varepsilon^2 \cos 2\omega_o t,$$

$$c_3 = \bar{c}_3 + \tilde{c}_3 \varepsilon \cos \omega_o t, \tag{28}$$

with

$$\bar{c}_2 = \rho A_i \bar{U}_i^2 (1 + \varepsilon^2/2) + \chi \rho A_o U_e^2, \qquad \tilde{c}_2^1 = 2\rho A_i \bar{U}_i^2,$$

$$\tilde{c}_2^2 = \rho A_i \bar{U}_i \omega_o, \qquad \tilde{c}_2^3 = \rho A_i \bar{U}_i^2/2,$$

$$\bar{c}_3 = 2\rho A_i \bar{U}_i + 2\chi \rho A_o U_e, \qquad \tilde{c}_3 = 2\rho A_i \bar{U}_i,$$

and obtain the following governing partial differential equation:

$$c_1 \frac{\partial^4 y}{\partial x^4} + (\bar{c}_2 + \tilde{c}_2^1 \varepsilon \cos \omega_o t + (x - l)\tilde{c}_2^2 \varepsilon \sin \omega_o t + \tilde{c}_2^3 \varepsilon^2 \cos 2\omega_o t) \frac{\partial^2 y}{\partial x^2}$$

$$+ (\bar{c}_3 + \tilde{c}_3 \varepsilon \cos \omega_o t) \frac{\partial^2 y}{\partial x \partial t} + c_4 \frac{\partial^2 y}{\partial t^2} = 0. \tag{29}$$

We express the solution of (29) in the form of a series

$$y(x,t) = \sum_{j=1}^{\infty} a_j(t)\,\phi_j(x), \tag{30}$$

where ϕ_j is the jth eigenfunction corresponding to eigenvalue λ_j for the system

$$\frac{\mathrm{d}^4\phi_j}{\mathrm{d}x^4} = \lambda_j^4\phi_j, \quad 0 < x < l, \tag{31}$$

with the boundary conditions

$$\phi_j(0) = \phi_j'(0) = 0,$$
$$\phi_j''(l) = \phi_j'''(l) = 0.$$

Moreover, the eigenvalue λ_j satisfies the transcendental algebraic equation (Blevins 1979)

$$1 + \cos\lambda_j l \cosh\lambda_j l = 0, \quad j = 1, 2, \ldots \tag{32}$$

and the corresponding ϕ_j is given by

$$\phi_j(x) = (\cos\lambda_j x - \cosh\lambda_j x) + \sigma_j(\sin\lambda_j x - \sinh\lambda_j x),$$
$$\sigma_j = (\sin\lambda_j l - \sinh\lambda_j l)/(\cos\lambda_j l + \cosh\lambda_j l). \tag{33}$$

Of course, we also have the following orthogonal relations:

$$\int_0^l \phi_j(x)\,\phi_k(x)\,\mathrm{d}x = 0, \qquad \int_0^l \phi_j''(x)\,\phi_k''(x)\,\mathrm{d}x = 0, \quad j \neq k. \tag{34, 35}$$

Substituting equation (30) into (29), multiplying the resulting equation by $\phi_k(x)$, and integrating from $x = 0$ to $x = l$, we obtain the following equation:

$$c_4\ddot{a}_k + \sum_{j=1}^{\infty} \{(\bar{c}_3 + \tilde{c}_3\varepsilon\cos\omega_o t)o_{kj}\dot{a}_j + (\bar{c}_2 + \tilde{c}_2^1\varepsilon\cos\omega_o t + \tilde{c}_2^3\varepsilon^2\cos 2\omega_o t)p_{kj}a_j + \tilde{c}_2^2\varepsilon q_{kj}a_j\sin\omega_o t\} + c_1\lambda_k^4 a_k = 0, \tag{36}$$

where

$$\mu_k = \int_0^l \phi_k^2\,\mathrm{d}x, \qquad o_{kj} = \int_0^l \phi_k\phi_j'\,\mathrm{d}x/\mu_k,$$
$$p_{kj} = \int_0^l \phi_k\phi_j''\,\mathrm{d}x/\mu_k, \qquad q_{kj} = \int_0^l (x-l)\,\phi_k\phi_j''\,\mathrm{d}x/\mu_k. \tag{37}$$

Notice that some analytical expressions exist for expressions (37), but in this work we choose to use numerical integrations. As in Ginsberg (1973), we select a two-term series expansion in (30), i.e., $j = 1, 2$. In this manner, we obtain the coupled equations for $a_1(t)$ and $a_2(t)$, which from equation (36) result in the following:

$$c_4\ddot{a}_1 + (\bar{c}_3 + \tilde{c}_3\varepsilon\cos\omega_o t)(o_{11}\dot{a}_1 + o_{12}\dot{a}_2) + (\bar{c}_2 + \tilde{c}_2^1\varepsilon\cos\omega_o t + \tilde{c}_2^3\varepsilon^2\cos 2\omega_o t)(p_{11}a_1 + p_{12}a_2) + \tilde{c}_2^2\varepsilon\sin\omega_o t(q_{11}a_1 + q_{12}a_2) + c_1\lambda_1^4 a_1 = 0, \tag{38}$$

$$c_4\ddot{a}_2 + (\bar{c}_3 + \tilde{c}_3\varepsilon\cos\omega_o t)(o_{21}\dot{a}_1 + o_{22}\dot{a}_2) + (\bar{c}_2 + \tilde{c}_2^1\varepsilon\cos\omega_o t + \tilde{c}_2^3\varepsilon^2\cos 2\omega_o t)(p_{21}a_1 + p_{22}a_2) + \tilde{c}_2^2\varepsilon\sin\omega_o t(q_{21}a_1 + q_{22}a_2) + c_1\lambda_2^4 a_2 = 0. \tag{39}$$

The coefficients in (38) and (39) are periodic with the period T_o and the transition from stability to instability is marked by the existence of a solution with the period T_o or $2T_o$.

The solutions associated with the primary instability at $\omega_o/\omega_{oi} = 2/k,\ k = 1, 3, 5, \ldots$ correspond to solutions with the period $2T_o$ and are constructed from the Fourier series as

$$a_i(t) = \sum_{j=1,3,5,\ldots}^{\infty} \left\{ r_{ij} \cos \frac{1}{2} j\omega_o t + s_{ij} \sin \frac{1}{2} j\omega_o t \right\}, \quad i = 1, 2, \tag{40}$$

while solutions associated with the secondary instability at $\omega_o/\omega_{oi} = 2/k,\ k = 2, 4, 6, \ldots$ correspond to solutions with the period T_o and are constructed using the Fourier series:

$$a_i(t) = \frac{1}{2} e_{i0} + \sum_{j=2,4,6,\ldots}^{\infty} \left\{ e_{ij} \cos \frac{1}{2} j\omega_o t + f_{ij} \sin \frac{1}{2} j\omega_o t \right\}, \quad i = 1, 2. \tag{41}$$

The primary principal instability boundary is generated by solutions of the form (40) with $j = 1$. Thus, truncating the series in equation (40), as in Ginsberg (1973), we have

$$a_i(t) = r_i \cos \frac{1}{2} \omega_o t + s_i \sin \frac{1}{2} \omega_o t, \quad i = 1, 2 \tag{42}$$

with $r_i \equiv r_{i1}$ and $s_i \equiv s_{i1}$. Substituting equation (42) into (38) and (39), using various trigonometric relations, and collecting the coefficients of the linearly independent terms $\sin 1/2\ \omega_o t$ and $\cos 1/2\ \omega_o t$, we obtain the system of algebraic equations

$$\begin{bmatrix} M_{11} & M_{12} & M_{13} & M_{14} \\ M_{21} & M_{22} & M_{23} & M_{24} \\ M_{31} & M_{32} & M_{33} & M_{34} \\ M_{41} & M_{42} & M_{43} & M_{44} \end{bmatrix} \begin{Bmatrix} r_1 \\ s_1 \\ r_2 \\ s_2 \end{Bmatrix} = \begin{Bmatrix} 0 \\ 0 \\ 0 \\ 0 \end{Bmatrix}, \tag{43}$$

where

$$M_{11} = -c_4\omega_o^2/4 + \bar{c}_2 p_{11} + \varepsilon\tilde{c}_2^1 p_{11}/2 + c_1\lambda_1^4, \qquad M_{12} = \bar{c}_3 o_{11}\omega_o/2 + \varepsilon\tilde{c}_3 o_{11}\omega_o/4 + \varepsilon\tilde{c}_2^2 q_{11}/2,$$

$$M_{13} = \bar{c}_2 p_{12} + \varepsilon\tilde{c}_2^1 p_{12}/2, \qquad M_{14} = \bar{c}_3 o_{12}\omega_o/2 + \varepsilon\tilde{c}_3 o_{12}\omega_o/4 + \varepsilon\tilde{c}_2^2 q_{12}/2,$$

$$M_{21} = -\bar{c}_3 o_{11}\omega_o/2 + \varepsilon\tilde{c}_3 o_{11}\omega_o/4 + \varepsilon\tilde{c}_2^2 q_{11}/2,$$

$$M_{22} = -c_4\omega_o^2/4 + \bar{c}_2 p_{11} - \tilde{c}_2^1 p_{11}/2 + c_1\lambda_1^4,$$

$$M_{23} = -\bar{c}_3 o_{12}\omega_o/2 + \varepsilon\tilde{c}_3 o_{12}\omega_o/4 + \varepsilon\tilde{c}_2^2 q_{12}/2, \qquad M_{24} = \bar{c}_2 p_{12} - \tilde{c}_2^1 p_{12}/2,$$

$$M_{31} = \bar{c}_2 p_{21} + \varepsilon\tilde{c}_2^1 p_{21}, \qquad M_{32} = \bar{c}_3 o_{21}\omega_o/2 + \varepsilon\tilde{c}_3 o_{21}\omega_o/4 + \varepsilon\tilde{c}_2^2 q_{21}/2,$$

$$M_{33} = -c_4\omega_o^2/4 + \bar{c}_2 p_{22} + \varepsilon\tilde{c}_2^1 p_{22}/2 + c_1\lambda_2^4, \qquad M_{34} = \bar{c}_3 o_{22}\omega_o/2 + \varepsilon\tilde{c}_3 o_{22}\omega_o/4 + \varepsilon\tilde{c}_2^2 q_{22}/2,$$

$$M_{41} = -\bar{c}_3 o_{21}\omega_o/2 + \varepsilon\tilde{c}_3 o_{21}\omega_o/4 + \varepsilon\tilde{c}_2^2 q_{21}/2, \qquad M_{42} = \bar{c}_2 p_{21} - \varepsilon\tilde{c}_2^1 p_{21}/2,$$

$$M_{43} = -\bar{c}_3 o_{22}\omega_o/2 + \varepsilon\tilde{c}_3 o_{22}\omega_o/4 + \varepsilon\tilde{c}_2^2 q_{22}/2,$$

$$M_{44} = -c_4\omega_o^2/4 + \bar{c}_2 p_{22} - \varepsilon\tilde{c}_2^1 p_{22}/2 + c_1\lambda_2^4.$$

The existence of the solution of the form (42) corresponds to $\det M_{ij} = 0$. Using this criterion, we may obtain the dynamic stability information associated with various design

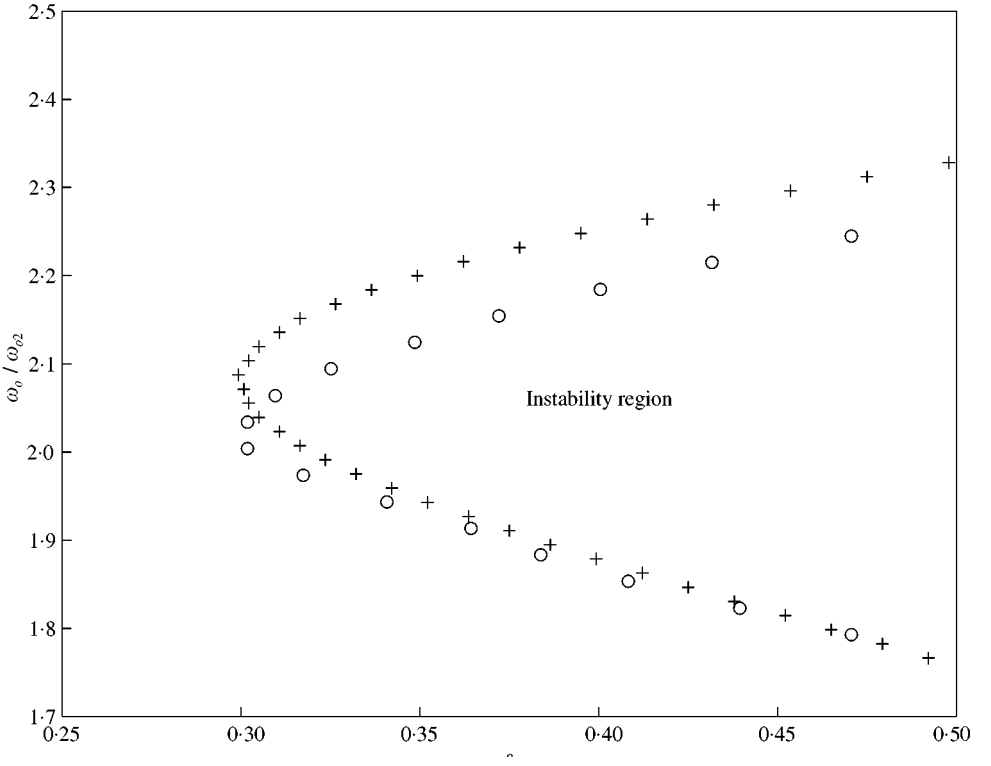

Figure 8. Results derived from the Floquet theory and the Bolotin method. (Eleven grid points for spatial discretization.) + , Bolotin method; ○, Floquet theory.

parameters, such as ε and ω_o. Figure 8 shows that the results derived from the Bolotin method and the Floquet theory match. The explanation for the 10% difference in Figure 8 might be attributed to the limited number of terms in the series expansion, which in this case is 2. It is also suggested by Figure 8 that the higher the excitation frequency the less accurate the Bolotin method becomes. This observation in fact is very much consistent with the fact that, to have the same accuracy, for higher frequencies, more terms of series expansion must be used.

The advantage of using the Bolotin method is, of course, its simplicity and efficiency; however, when considering more terms in the series expansions, a derivation based on the Bolotin method can be extensive, and in addition, the Bolotin method is limited to the parametric instability analysis (Païdoussis & Sundararajan 1975).

6. CONCLUSIONS

Based on the mathematical model for a submerged concentric pipe system with both unconfined and confined external flows, we have studied both static and dynamic stability issues related to the pipe system design. We have presented the ranges of both buckling and flutter instability for pipes conveying steady flows for a case study. For the pipes conveying pulsatile fluids, we have also presented two methods to determine the regions of dynamic instability. We find that the outer pipe length is a more important design factor than gravity (relating to inclination angle and submergence depth) and friction. For the inner pipe

conveying pulsatile flow, the lowest critical perturbation frequency is nearly twice the second system's natural frequency. However, we note that for current pipe system designs with reasonable flow rates, the concentric pipe system is stable. The procedure implemented in this paper clearly shows much promise in assisting the design for the silo piping system.

ACKNOWLEDGEMENTS

The authors would like to thank the Institute of Paper Science and Technology and its Member Companies for their support.

APPENDIX: NOMENCLATURE

A cross-sectional area of the tubular beam, $\pi(R_o^2 - R_i^2)$
A_i inner cross-sectional area of the tubular beam, πR_i^2
A_o outer cross-sectional area of the tubular beam, πR_o^2
D_o outer diameter of the inner pipe
E elastic modulus of the pipe
g gravity
I area moment of the tubular beam, $\pi(R_o^4 - R_i^4)/4$
l inner pipe length
L outer pipe length
p_i internal pipe pressure
p_e external pipe pressure
R_e inner radius of the outer pipe
R_i inner radius of the tubular beam
R_o outer radius of the tubular beam
T axial tension
U_e averaged turbulent flow velocity for the external pipe flow
U_i averaged turbulent flow velocity for the internal pipe flow
x_o entrance distance associated with the turbulent boundary layer

Greek letters
ε internal pipe flow velocity perturbation
θ inclination angle
ρ internal and external fluid densities

REFERENCES

ARIARATNAM, S. T. & NAMACHCHIVAYA, N. S. 1986 Dynamic stability of pipes conveying pulsating fluid. *Journal of Sound and Vibration* **107,** 215–230.

ASHLEY, H. & HAVILAND, G. 1950 Bending vibrations of a pipe line containing flowing fluid. *Journal of Applied Mechanics* **17**, 229–232.

BATHE, K. J. 1996 *Finite Element Procedures*. Englewood Cliffs, NJ: Prentice-Hall.

BENJAMIN, T. B. 1961*a* Dynamics of a system of articulated pipes conveying fluid. I. Theory. *Proceedings of the Royal Society Series A*, **261,** 457–486.

BENJAMIN, T. B. 1961*b* Dynamics of a system of articulated pipes conveying fluid. II. Experiments. *Proceedings of the Royal Society Series A*, **261**, 487–499.

BLEVINS, R. D. 1979 *Formulas for Natural Frequency and Mode Shape*. New York: Van Nostrand Reinhold.

BOLOTIN, V. V. 1964 *The Dynamic Stability of Elastic Systems*. San Francisco: Holden-Day.

CHEN, S. S. 1971 Dynamic stability of tube conveying fluid. *ASCE Journal of the Engineering Mechanics Division* **97,** 1469–1485.

GINSBERG, J. H. 1973 The dynamic stability of a pipe conveying a pulsatile flow. *International Journal of Engineering Science* **11,** 1013–1024.
HANNOYER, M. J. & PAÏDOUSSIS, M. P. 1978 Instabilities of tubular beams simultaneously subjected to internal and external axial flows. *ASME Journal of Mechanical Design* **100,** 328–336.
NOAH, S. T. & HOPKINS, G. R. 1980 Dynamic stability of elastically supported pipes conveying pulsating fluid. *Journal of Sound and Vibration* **71,** 103–116.
PAÏDOUSSIS, M. P. 1966 Dynamics of flexible slender cylinders in axial flow. Part 1. Theory. *Journal of Fluid Mechanics*, **26,** 717–736.
PAÏDOUSSIS, M. P. 1973 Dynamics of cylindrical structures subjected to axial flow. *Journal of Sound and Vibration*, **29,** 365–385.
PAÏDOUSSIS, M. P. 1998 *Fluid-Structure Interactions—Slender Structures and Axial Flow*. London: Academic Press.
PAÏDOUSSIS, M. P. & ISSID, N. T. 1974 Dynamic stability of pipes conveying fluid. *Journal of Sound and Vibration* **33,** 267–294.
PAÏDOUSSIS, M. P. & LI, G. X. 1993 Pipes conveying fluid: a model dynamical problem. *Journal of Fluids and Structures* **7,** 137–204.
PAÏDOUSSIS, M. P. & PETTIGREW, M. J. 1979 Dynamics of flexible cylinders in axisymetrically confined axial flow. *Journal of Applied Mechanics* **46,** 37–44.
PAÏDOUSSIS, M. P. & SUNDARARAJAN, C. 1975 Parametric and combination resonances of a pipe conveying pulsating fluid. *Journal of Applied Mechanics* **42,** 780–783.
SCHLICHTING, H. 1987 *Boundary-Layer Theory*, 7th edition. New York: McGraw-Hill.
TAYLOR, G. 1952 Analysis of the swimming of long and narrow animals. *Proceedings of the Royal Society Series A*, **214,** 158–183.
WANG, X. & BLOOM, F. 1999 Dynamics of a submerged and inclined concentric pipe system with internal and external flows. *Journal of Fluids and Structures* **13,** 443–460.
WANG, X., FENG, Z. & FORNEY, L. J. 1999 Computational simulation of turbulent mixing with mass transfer. *Computers & Structures* **70,** 447–465.
WANG, X. & HALE, J. K. 2001 On monodromy matrix computation. *Computer Methods in Applied Mechanics and Engineering*, **190,** 2263–2275.
ZIENKIEWICZ, O. C. 1977 *The Finite Element Method*, 3rd edition. New York: McGraw-Hill.